Stochastic Environmental Research and Risk Assessment (2026) 40:24
https://doi.org/10.1007/s00477-025-03159-x

ORIGINAL PAPER

Spatio-temporal analysis of record-breaking temperature increments across Spain

Ana C. Cebrián[1] · Jesús Asín[1] · Jorge Castillo-Mateo[1] · Alan E. Gelfand[2]

Received: 1 September 2025 / Accepted: 9 October 2025

Abstract
The study of record-breaking values is of significant interest in environmental sciences. Studying records implies analyzing *both* their occurrence and their magnitude. Further, the study of this phenomenon within a spatio-temporal framework is vital for evaluating seasonal behaviors, identifying spatial patterns, and quantifying the effect of climate change on it. With interest in record-breaking temperatures, we specify models for these observations rather than models for the entire daily temperature stream. Models specifically designed for record-breaking events must consider two random components: the occurrence and the magnitude of each record. With primary interest in the magnitudes, we model the magnitude data *given* the occurrence data, with the goal of making inference about their evolution within a spatio-temporal framework. We employ a set of 40 geo-referenced time series of daily temperatures across peninsular Spain. From these, we extract the series of occurrences and values of record-breaking events during the summer months, June, July, and August, spanning from 1960 to 2021. The results reveal that the behavior of the increments is neither spatially nor temporally homogeneous, and that there is significant dependence on the previous day: the occurrence of a record increases the posterior mean of the next day's increment by between 0.3 and 0.6 °C. It is also found that the posterior mean of the average increment on a record-breaking day during the decade 2012–2021 is approximately 1 °C inland, increasing to around 2°C in some coastal areas. After 30 years, mean increments stabilize near 1°C with a mild downward trend.

Keywords Bayesian hierarchical model · Conditional model · INLA · Record-breaking temperatures · Record-breaking values · Space-time model

1 Introduction

The study of record-breaking values is of significant interest in environmental sciences, especially in areas such as wave height, flood levels, wind speed, climate studies related to precipitation Lehmann et al. (2015, 2018) and, most notably, temperature (Newman et al. 2010; Wergen et al. 2014; Sousa et al. 2019; Jiang et al. 2024). Temperature data, and consequently their record-breaking events, can be analyzed across various time scales; however, the most significant impacts on human health and biodiversity are associated with heatwaves, which are defined and measured at the daily scale (Yang et al. 2024; Tian et al. 2025). Therefore, in this work we focus on this time scale and, specifically, on calendar-day records, i.e., the record-breaking events in each time series corresponding to each day of the year, across years; see Elguindi et al. (2013) and Pan et al. (2013) for further discussion of the advantages of using calendar day records in climate studies.

Formal investigation of record-breaking events implies analyzing *both* their occurrence and their value. Castillo-Mateo et al. (2025) presented a spatio-temporal model for the *occurrence* of record-breaking events, including complex dependence structures. However, to the best of our knowledge, no spatio-temporal modeling of the *values* of record-breaking events, whether for temperature or other variables, has been presented in the literature. The aim of this work is to fill that gap. Moreover, instead of modeling the record values directly, we propose an approach that models the increments relative to the previous record value,

✉ Ana C. Cebrián
acebrian@unizar.es

[1] Departamento de Métodos Estadísticos, Universidad de Zaragoza, Zaragoza, Spain

[2] Department of Statistical Science, Duke University, Durham, NC, USA

Published online: 13 January 2026

conditional on a record-breaking event having occurred (i.e., positive increments). This approach is simpler to implement since increments can be treated as conditionally independent, whereas record values are subject to a left censoring order constraint. In addition, increments offer a consistent basis for comparison across sites and time periods by removing site-specific baselines, much like the temperature anomalies used in climate studies. Note that by focusing on positive increments, we can confine ourselves to conditional modeling, i.e., modeling the increment given that a record has occurred.

Using this model, we aim to address key climate-related questions, such as evaluating trends in record values over time, examining differences within the summer months, identifying factors that influence record-breaking temperatures, and assessing the presence of serial correlation. We also investigate these issues spatially, both to assess spatial dependence and variation, and to characterize annual trends across regions with different environmental characteristics. Modeling within a hierarchical Bayesian spatio-temporal framework enables us to obtain full posterior predictive distributions to address the following questions, and to quantify the associated uncertainty: (i) Do we observe differences in seasonal behavior? (ii) Can we identify spatial patterns? (iii) Can we detect decadal temporal patterns to quantify the effects of climate change on record-breaking temperatures? (iv) Is there an effect of a previous day's record-breaking event on increments? (v) Can we predict increment behavior at unobserved locations? The answers to these questions will be of significant value to the climate research community.

Another question of interest in climate research is to quantify the deviation of the observed behavior of record-breaking temperatures from what would be expected under a stationary climate, i.e., in i.i.d. sequences. To this end, it is useful to exploit the probabilistic properties of record-breaking events in i.i.d. series. For the occurrence of record-breaking events, these properties are simple and distribution-free, making such comparisons straightforward (Castillo-Mateo et al. 2025). Unfortunately, for the values of the records, the properties are more complex. The distribution of the increments of record-breaking values in i.i.d. sequences depends on the underlying distribution of the sequence (Arnold et al. 1998, Section 2.10), and therefore general distribution-free results are not available. Some analytical results exist for specific distributions, such as the exponential, Pareto, Weibull, and extreme value distributions (Arnold et al. 1998, Chapter 3), but they are not applicable in our context.

Here, models are fitted within a Bayesian framework, which allows us to incorporate dependence over time and space using relevant covariates and random effects. Additionally, the Bayesian framework provides *generative* models, which enable us to propose a Monte Carlo (MC) approach to validate them and draw inference from them. Specifically, this MC approach serves as a powerful tool for making inferences about arbitrary characteristics of interest of the distribution of the records and, as a result, addressing the research questions of interest.

It could be argued that one seemingly straightforward approach for analyzing calendar-day record-breaking temperature series would be to model the entire distribution of temperatures. A generative model for daily temperature could theoretically produce samples of record-breaking events, which can then be used to infer the distribution of the occurrence and magnitude of these records. However, developing a model that accurately represents the full range of daily temperatures, particularly the record-breaking events, presents significant challenges, especially within a spatio-temporal framework. Models designed to capture the entire temperature distribution tend to perform well in fitting the bulk of the distribution, where more data are available, but often perform poorly in the tails of the distribution (Keellings and Waylen 2015; Shaby et al. 2016). Additionally, these models will usually impose a single trend across both central and extreme values and will assume uniform seasonal effects and covariate influences. This assumption, however, is unrealistic (Schliep et al. 2021; Castillo-Mateo et al. 2023). That is the reason why models for extreme events focus on alternative approaches such as exceedance thresholds, block maxima, or specific quantiles (Coles 2001). Such models allow for a more flexible and accurate representation of the behavior of the tails.

Similarly, given that our interest is in temperatures associated with record-breaking, it seems more appropriate to confine ourselves to modeling temperature increments associated with these events. In what follows, we extract increment data associated solely with record-breaking events and we focus on models specifically for such data. Such a focus enables us to specify simpler models that achieve good explanatory and predictive performance. It is worth noting that our data is no longer a daily time series but rather a sequence of event times with an associated mark, a temperature increment.

The proposed approach is applied to a set of 40 geo-referenced time series of daily temperatures across peninsular Spain. From these, we extract the series of occurrences and values of record-breaking events during the three summer months, June, July, and August (JJA), spanning from 1960 to 2021. We model the increments of calendar-day records, i.e., the records for each day within the three-month window at each site, resulting in 92 yearly series per site.

The remainder of the manuscript is organized as follows. Section 2 presents the daily temperature data and an EDA of

the records. Section 3 describes the modeling framework for the increments introduced in this work. Section 4 introduces the specific structure of the proposed spatio-temporal models, outlines the selection process used to identify the most adequate model, and presents the final selected model. Once the best model is selected, Sect. 5 presents validation tools to assess its adequacy, and Sect. 6 reports post-model inference results obtained via MC simulation based on the conditional and marginal distributions of the increments provided by the final model. Finally, Sect. 7 concludes with a summary and directions for future research. Additional details and graphics are provided in the Supplementary Material.

2 Data and exploratory analysis

2.1 Data and study area

The study area is peninsular Spain, defined as the region of Spain within the Iberian Peninsula, covering approximately 492,175 km^2. The dataset is point-referenced to a collection of monitoring stations and includes daily maximum temperature observations from January 1, 1960, to December 31, 2021. Specifically, it is extracted from the European Climate Assessment & Dataset (ECAD; Klein Tank et al. 2002), spanning 40 weather stations. The Spanish temperature series available in ECAD are provided by AEMET and are measured to the nearest $1/10\,^{\circ}$C.

For analyses focused on daily temperature record indicators across years, the dataset is organized into 365 binary series (with February 29 removed for convenience) of length 62 for each site. In this study, we consider only the 92 series corresponding to the days in JJA. Figure 1 shows the locations of the stations within the Iberian Peninsula. Spain is geographically diverse, featuring several mountain ranges such as the Pyrenees in the northeast, the Inner Plateau in the center, and the Sierra Nevada near the southern Mediterranean coast. The region has an extensive coastline bordered by the Atlantic Ocean to the north and west, and the Mediterranean Sea to the south and east.

The stations are irregularly distributed across Spain in an effort to represent its varied climatic zones. The stations also span a wide range of elevations, including five located above 800 m, and 16 situated along the coast. The stations considered in this study have a negligible amount of missing data, with an average missing rate of 0.07%. It is assumed that no record-breaking observations occurred on those days; a simulation study conducted by Castillo-Mateo et al. (2025) using the same dataset showed that the missing data had a negligible impact on the results. To summarize, the dataset used to fit the model consists of the record increments, $J_{t\ell}(\mathrm{s}_i)$, where $\ell \in \mathcal{L} = \{1, \ldots, 92\}$ corresponds to days from June 1 to August 31, $t \in \mathcal{T} = \{2, \ldots, 62\}$ represents years from 1961 to 2021, and $\mathrm{s}_i \in \mathcal{S} = \{\mathrm{s}_1, \ldots, \mathrm{s}_{40}\}$ are the geographic coordinates for the 40 weather stations.

2.2 Exploratory analysis of record increment values

An exploratory data analysis (EDA) is conducted to identify the key features for inclusion in the model. To achieve this, we compute and plot the empirical densities of record increments across different time periods and conditions; the

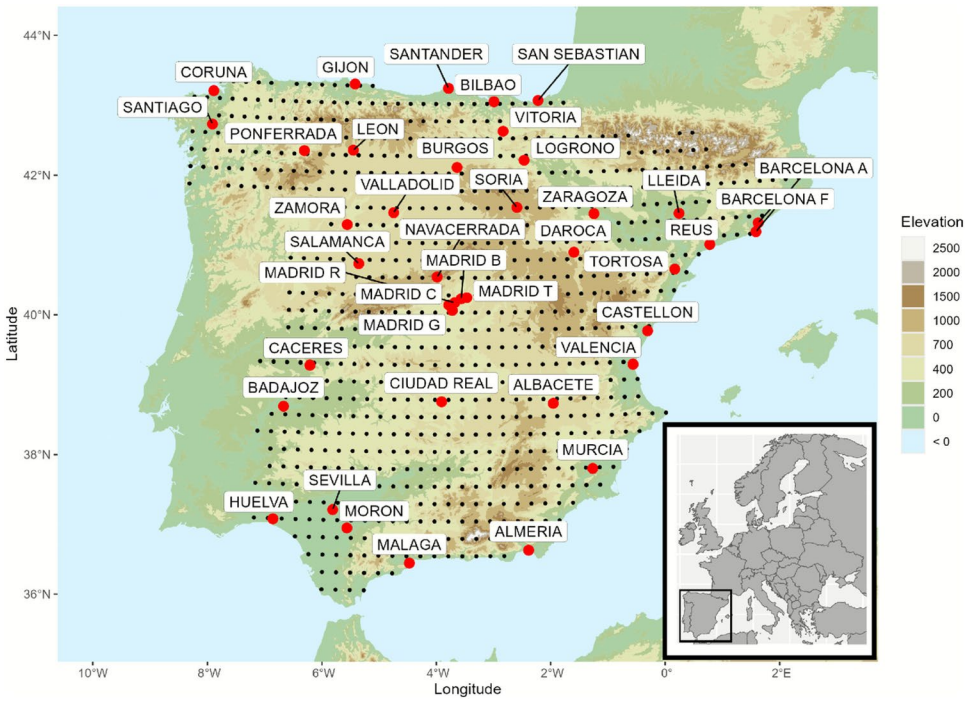

Fig. 1 Map of the 40 Spanish stations (red points), and the prediction grid (black points)

densities are estimated using the Beta boundary kernel by Chen (1999) for positive variables. This section presents the results that highlight the most relevant features.

Probability distribution and decadal evolution Figure 2 (left) presents the empirical densities for 10-year periods (except for the first one, which covers 1961–1971), obtained from all stations. The shape of the empirical density in each period suggests that a Gamma distribution may be appropriate. Notably, the mode of the empirical density is far from zero in all cases, indicating that a simpler distribution, such as the Exponential distribution, will not be adequate. A temporal evolution is observed, with the early years exhibiting greater variability than the later period, as expected from record behavior.

Previous day effect Due to the strong serial correlation in daily temperature, a record occurrence on previous days may influence the increment value. Figure 2 (right) presents the empirical density of increments when the previous day was a record versus when it was not, for the last decade. The increments tend to be higher when the previous day was a record. This effect appears stable over time, as a similar pattern is observed in the 1992–2001 period.

Seasonal behavior The behavior of increments is not homogeneous within the JJA period and the monthly distributions vary across decades, see the plots in Section 1 of the Supplementary Material.

Spatial variability It is well known that elevation influences temperature-related variables, but other geographical factors, such as coastal proximity, may also play a role. To investigate this effect, we compare the empirical density of increments for stations located within 50 km of the coast versus those farther inland, revealing distinct distributions. Furthermore, this difference depends on whether a record occurred the previous day or not, see the plots in Section 1 of the Supplementary Material.

In summary, the EDA suggests that a Gamma distribution is appropriate for modeling the increments. The results further indicate that the distribution varies across days, years, and space, particularly as a function of distance to the coast, and that there is dependence on the previous day, which also varies with distance to the coast. Consequently, the model should consider the inclusion of trend and seasonal terms, the effect of the previous day, the influence of distance to the coast, and the necessary interactions among these components.

3 Modeling structure of the increments

The modeling structure for this problem presents some methodological challenges. Let t denote years, ℓ days within years, and s_i observed sites, with the set of all observed combinations of years, days, and sites defined as $\mathcal{A} = \mathcal{T} \times \mathcal{L} \times \mathcal{S}$. To explain the positive increments (or jumps), i.e., the set $\mathrm{J} = \{J_{t\ell}(\mathrm{s}_i) : (t, \ell, \mathrm{s}_i) \in \mathcal{A}\}$, we need the set of indicator variables $\mathrm{I} = \{I_{t\ell}(\mathrm{s}_i) : (t, \ell, \mathrm{s}_i) \in \mathcal{A}\}$, where $I_{t\ell}(\mathrm{s}_i)$ indicates whether a record-breaking temperature occurred in year t on day ℓ at site s_i, i.e., whether the temperature on that specific day and location exceeds all previous observations for the same calendar day at that site. Since I may serve as a regressor in explaining J, and because it is stochastic, we need to model increments conditional on these indicators. Furthermore, our goal is to model only the positive increments, i.e., the values $J_{t\ell}(\mathrm{s})$ associated with $I_{t\ell}(\mathrm{s}) = 1$. Given that I is observed, we therefore consider the conditional distribution $\mathrm{J} \mid \mathrm{I}$. For simplicity, we will refer to these positive increments simply as *increments*.

As we demonstrated in the previous section, a critical predictor in explaining $J_{t\ell}(\mathrm{s})$ is $I_{t,\ell-1}(\mathrm{s})$, i.e., whether or not there was a record-breaking event on the previous day. Thus, we cannot consider only $I_{t\ell}(\mathrm{s}) = 1$, and instead must retain the conditional structure $\mathrm{J} \mid \mathrm{I}$ in our modeling. However, this reveals an awkward prediction challenge. To make prediction of the increments at unobserved sites using the

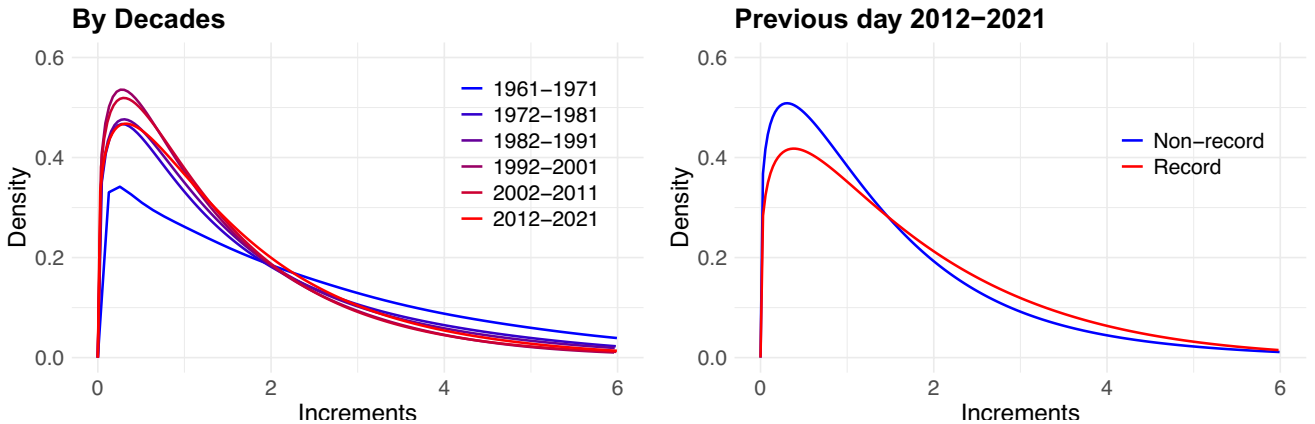

Fig. 2 Empirical density of the record increments, in °C, per periods across time (left), and conditioned on the occurrence of a record the previous day in last decade (right)

regression model, we will assume that the indicator for that year, day, and location is 1. However, we will need the previous day indicator and this will not be known.

There are several alternatives within a hierarchical Bayesian framework. The first is to present two posterior predictive distributions, one given the previous day indicator was equal to 1 and one when it was equal to 0. Comparison of these two distributions will be informative in assessing how the previous day's information influences the distribution of the increment.

Further, we can also consider the marginal posterior predictive distribution, which does not require specification of the previous day's indicator. We can obtain this as a mixture distribution using mixture weights that provide the probability for the previous day's indicator to be equal to 1 and therefore, equal to 0. An elementary choice would arise from the classical stationary record-breaking model (Arnold et al. 1998, Chapter 2) where, the probability of record at time t is $1/t$, but this is not a reasonable assumption under global warming. If we adopt a parametric model for record breaking, e.g., a linear drift model (Rahmstorf and Coumou 2011; Coumou et al. 2013) or a fully developed spatial record-breaking model, as in Castillo-Mateo et al. (2025), then the probability for the previous day's indicator to equal 1 is a parametric function, a random variable in the Bayesian setting. With a posterior distribution for this probability, we obtain a posterior distribution for the marginal predictive distribution. A convenient summary of this predictive distribution is the posterior mean that can be obtained by averaging with the posterior mean probability that the previous day's indicator is equal to 1 as well as 0; note that these probabilities of record can be readily estimated, either by the simplistic empirical proportions of records or by more sophisticated estimation techniques.

4 A space-time model for record-breaking increments in daily maximum temperatures

Increments are positive and asymmetric quantities, so that a Gamma distribution may be an appropriate model. This assumption is further supported by the EDA in Section 2.2; see the empirical density estimators in Fig. 2 and the accompanying comments. Consequently, it is assumed that $J_{t\ell}(\mathrm{s}) \mid I_{t\ell}(\mathrm{s}) = 1$ follows a Gamma distribution with the following density function:

$$f_{J_{t\ell}(\mathrm{s})}(y) = \left(\frac{\phi}{\mu_{t\ell}(\mathrm{s})}\right)^{\phi} \frac{1}{\Gamma(\phi)} y^{\phi-1} \exp\left(-\frac{\phi y}{\mu_{t\ell}(\mathrm{s})}\right), \quad y > 0,$$

where $\phi > 0$ is a constant shape parameter, $\mu_{t\ell}(\mathrm{s}) > 0$ is the mean and $\mathrm{var}\,(J_{t\ell}(\mathrm{s})) = \mu_{t\ell}(\mathrm{s})^2/\phi$. The logarithm of the mean is modeled as a linear predictor,

$$\log(\mu_{t\ell}(\mathrm{s})) = \eta_{t\ell}(\mathrm{s}) = \beta_0 + \mathrm{Z}_{t\ell}^{\top}(\mathrm{s})\boldsymbol{\beta} + w_{t\ell}(\mathrm{s}).$$

Here, β_0 is a global intercept, $\mathrm{Z}_{t\ell}(\mathrm{s})$ denotes a column vector of spatial and temporal covariates, $\boldsymbol{\beta}$ denotes the corresponding column vector of regression coefficients, and $w_{t\ell}(\mathrm{s})$ is a component of random effects.

The models are fitted using `R-INLA` (Rue et al. 2024). In order to properly define the time dependencies, `R-INLA` requires the use of a complete time series, with time points where a record-breaking temperature has not occurred are filled with `NA` values. More details on the fit of the model and the priors used in the estimation can be found in Section 2 of the Supplementary Material, and details on the INLA methodology in Rue et al. (2009).

The remainder of this section first describes the procedure used to select the covariates which are relevant for modeling the increments. Once the covariates in the linear predictor are fixed, we consider alternative specifications for the random effects to capture remaining dependence across time and space. Model selection is then carried out using two in-sample criteria and a simple out-of-sample metric. Finally, the key output of the final selected model is presented.

4.1 Selecting the covariates

The EDA identified a set of covariates that appear to influence the value of the increments. The need to include these covariates in the model was assessed using 95% credible intervals (CIs) obtained from a model without random effects. After the selection procedure, the final set of covariates included in the model are: $\log(t)$ and its square, which capture the annual trend, geographical variables such as the logarithm of elevation, $\mathrm{logElev}\,(\mathrm{s})$, and distance to the coast, $\mathrm{logDC}\,(\mathrm{s})$, measured in meters and kilometers respectively, and the interaction between the latter and $\log(t)$; to avoid undefined values $\mathrm{logDC}\,(\mathrm{s})$ is defined as $\log(1 + DC(\mathrm{s}))$. To account for the serial correlation, a Markovian structure represented by the previous day's record indicator, $I_{t,\ell-1}(\mathrm{s})$, and its interaction with $\mathrm{logDC}\,(\mathrm{s})$ are also included. The interactions $\log(t) \times \mathrm{logDC}\,(\mathrm{s})$ and $I_{t,\ell-1}(\mathrm{s}) \times \mathrm{logDC}\,(\mathrm{s})$ allow the time trend and persistence to vary spatially. Given the differences observed across the three considered months, we explored including harmonic terms; however, they were not flexible enough to capture the complex behavior. Instead, seasonal differences will be captured using random effects as detailed below. Finally, due to the effect of large warm fronts that affect the entire peninsula and last for several days, joint spatio-temporal dependence is expected.

To capture this structure, we introduce a global covariate $I^{Sp}_{t,\ell-1}$ that provides the observed number of records in the previous day over all of the weather stations. The model including all these covariates is denoted *Model M1*.

Other covariates were considered, such as a function of the record position k, $\exp(-k)$, the time to the previous record occurrence, $\exp(-(t_k - t_{k-1}))$, and interactions of the lag record indicator and the year trend with $\log\text{Elev}\,(\mathrm{s})$; none of them were found significant.

4.2 Including random effects

Although both spatial and temporal covariates have been included in the model, they may not capture well enough dependence over time and across space. Therefore, in this section, we assess whether adding random effects to the previous model is necessary to capture the remaining dependence structure. To this end, we consider three options: MS1, which includes a spatially-varying intercept, and MS2 and MS3, which build on this intercept by adding different terms to capture potential temporal structure.

Model MS1. This model includes only a spatially-varying intercept, i.e., $w_{t\ell}(\mathrm{s}) = w(\mathrm{s})$. This term aims to capture spatial dependence and enables local adjustments to the global intercept, accounting for influences such as geographical characteristics not captured by the fixed effects. Spatial dependence is modeled using a SPDE approach, in which a Matérn Gaussian random field is approximated by discretizing the domain over a mesh and representing the field as a Gaussian Markov random field, resulting in a sparse precision matrix (Lindgren et al. 2022). The range and smoothness of the spatial correlation are governed by the SPDE parameters; see Section 2 of the Supplementary Material for more details.

Model MS2 This model considers annual intercepts that may capture a time trend potentially more complex than that modeled by the fixed effects, that is the covariates related to $\log(t)$. The resulting random effects are additive, taking the form,

$$w_{t\ell}(\mathrm{s}) = w(\mathrm{s}) + w_t,$$

where the annual intercepts are modeled as independent with $w_t \sim N(0, \sigma_1^2)$. We also considered modeling them using an AR(1) structure across years but the temporal dependence was found not to be significant.

Model MS3 This model assumes a more complex temporal structure represented by daily intercepts with a Markovian AR(1) structure. That is,

$$w_{t\ell}(\mathrm{s}) = w(\mathrm{s}) + w_{t\ell}, \quad \text{with } w_{t\ell} = \rho w_{t,\ell-1} + \epsilon_{t\ell}, \qquad (1)$$

where $\epsilon_{t\ell} \sim N(0, \sigma_\epsilon^2)$ are independent Gaussian errors. These temporal terms account for serial correlation between days not explained by the autoregressive covariates, as well as interannual variations in seasonal behavior, as indicated by the EDA; see Section 2 of the Supplementary Material for details on the autoregressive structure.

More complex random effects were tried, including a term represented by a latent spatio-temporal process which changes in time with first-order autoregressive dynamics and spatially correlated errors. However, these additions did not improve model performance.

4.3 Model comparison and selection

Model selection among M1, MS1, MS2 and MS3 is performed employing three different metrics. First, an in sample comparison is implemented using the deviance information criterion (DIC) and the root mean square error

$$\mathrm{RMSE} = \sqrt{\frac{1}{N} \sum_{(t,\ell,\mathrm{s}_i)\in\mathcal{A}_1} \left[J_{t\ell}(\mathrm{s}_i) - post\_mean(J_{t\ell}(\mathrm{s}_i))\right]^2},$$

where $\mathcal{A}_1 = \{(t, \ell, \mathrm{s}_i) \in \mathcal{A} : I_{t\ell}(\mathrm{s}_i) = 1\}$ denotes the set of days and sites with a record, and $N = \sum_{(t,\ell,\mathrm{s}_i)\in\mathcal{A}} I_{t\ell}(\mathrm{s}_i)$ is its size, i.e., the total number of records observed in the 92×40 series across 62 years considered, excluding the first trivial year.

The third comparative metric is an out-of-sample spatial evaluation using RMSE and a 10-fold testing scheme. In each iteration, the model is fitted while excluding data from four sites. Predictions and residuals for these excluded sites are then computed. This process is repeated 10 times, ensuring that each receives one out-of-sample prediction. Finally, RMSE_{os}, the RMSE from these predictions, is calculated.

Table 1 shows the three metrics used to compare and select the best model, DIC, RMSE and RMSE_{os}, for models M1, MS1, MS2, MS3 and a baseline model M0 with constant parameters. To demonstrate the need for a Gamma distribution, we also consider a *Model MS3exp*, which includes the same fixed and random effects in the linear predictor as model MS3 but with an Exponential distribution with parameter $\lambda_{t\ell}(\mathrm{s}) = 1/\mu_{t\ell}(\mathrm{s})$ where $\log(\mu_{t\ell}(\mathrm{s})) = \eta_{t\ell}(\mathrm{s})$. The improvement from including the covariates, model M1, is clear both in terms of the DIC and the RMSE. The same applies to model MS1, that incorporates a spatially varying intercept. Regarding temporal dependence, although model MS2, which includes annual random effects, improves performance, model MS3, incorporating daily effects with an autoregressive structure, performs even better, providing an improvement comparable to the inclusion of covariates. The

Table 1 DIC, and RMSE (in $^\circ C$) for models M1, MS1, MS2 and MS3 with a Gamma distribution and MS3 with an exponential distribution

	M0	M1	MS1	MS2	MS3	MS3exp
DIC	129,120	125,578	124,842	124,612	122,634	125,650
RMSE	2.00	1.80	1.75	1.73	1.51	2.87
RMSE_{os}	2.01	1.81	1.78	1.77	1.63	–

RMSE_{os} is only computed for models with a Gamma distribution

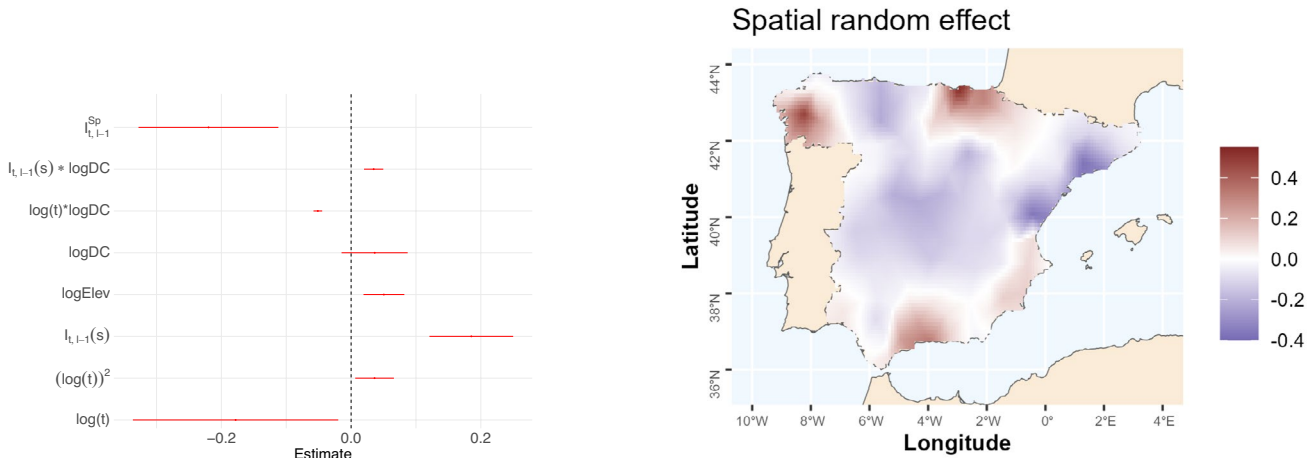

Fig. 3 Left: Posterior mean and 95% CI of the covariate coefficients in the model MS3. Right: Spatial random effects from the model MS3 over peninsular Spain

results for model MS3exp further confirm the benefit of a Gamma distribution over an Exponential one.

The spatial out-of-sample metric RMSE_{os} confirms the selection of model MS3 as the best model, with the inclusion of covariates and daily random effects providing the greatest improvement.

4.4 Description of the final selected model

Based on the previous results, our final selected model is MS3, a model with a Gamma distribution that includes eight covariates, a global and a spatially varying intercept, and daily effects with an autoregressive structure, see Equation 1. Figure 3 (left) summarizes the posterior mean and the 95% CIs for the eight covariate coefficients. Only the CI of $\text{logDC}\,(\text{s})$ includes zero, but this term is retained in the model since both interaction terms, $\log(t) \times \text{logDC}\,(\text{s})$ and $I_{t,\ell-1}(\text{s}) \times \text{logDC}\,(\text{s})$ are significant.

Regarding random effects, Fig. 3 (right) presents a map of the posterior mean of the spatial intercept, showing that many coastal areas, specifically the Basque Country and Galicia in the north, as well as the southeastern regions, exhibit an increase relative to the global intercept. With respect to the dependence on the previous day captured by the temporal random effect, the posterior mean of ρ is 0.58 with 95% CI (0.51, 0.63), suggesting that the autoregressive terms $I_{t,\ell-1}(\text{s})$ and $I_{t,\ell-1}(\text{s}) \times \text{logDC}\,(\text{s})$ account for only part of the existing serial dependence.

Finally, the posterior mean of the Gamma shape parameter ϕ is 1.8 with 95% CI (1.78, 1.86), which clearly does not include 1, the value corresponding to an Exponential distribution.

5 Adequacy of the final model MS3

This section presents validation and inference tools to assess the adequacy of the selected model MS3. These include an evaluation of the coverage of daily increments and comparisons between empirical averages of interest and the corresponding posterior means and CIs provided by the model. Specifically, we examine the proportion of increments below a given threshold (cumulative probabilities) and the spatial averages for selected years and days within the year. These tools rely on MC methods, which are feasible since MS3 can be employed as a generative model of daily increments. As additional validation tools, some graphical analyses of the residuals and fitted values are presented in Section 3 of the Supplementary Material.

5.1 Coverage of the daily increments

Coverage analysis is a useful tool for evaluating model adequacy. In our case, we assess the coverage of daily increments on days when a record is observed, using a hold out approach. For each of these days, we compute 95% CIs for

the increments, and then check whether the actual observed increment lies within the corresponding interval. As validation metrics, we report the overall average coverage as well as average coverage by year, by day of the year, and by site, to assess potential weaknesses in the model's ability to capture key characteristics.

To implement the hold out approach, the model is fitted excluding the series from 4 of the 40 available sites. Next, using the joint posterior distribution of all the parameters in the model, $B = 1000$ samples of the mean for each day, along with the shape hyperparameter of the distribution, are generated. These parameters are then used to generate B samples of increments for each day with an observed record in the four excluded sites, utilizing the distribution defined by the generated parameters. From these samples, a 95% CI for the increment on each day with a record is computed. To increase the sample size for computing validation metrics, this procedure is repeated 10 times, so that out-of-sample predictions are obtained for all sites. The same random sets of four locations used in Sect. 4.3 are applied here.

The average 95% coverage across all data is 0.93, indicating good model performance. The average coverage values for different years, days within the year, and sites are summarized in Section 4 of the Supplementary Material, and they indicate that the model effectively captures the evolution of increments over time. Similarly, the model captures seasonal patterns well, with most of the coverage values falling between 0.90 and 0.96, and seven values ranging from 0.85 to 0.90. The model also accounts for spatial variation adequately, although coverage falls between 0.80 and 0.90 at seven sites.

5.2 Analyzing cumulative probabilities

The previous MC approach can also be used to implement an out-of-sample validation of the model by comparing cumulative probabilities of the conditional distribution of the increments obtained from the model with their empirical counterparts. Specifically, for each site s_i in the sample, we consider the probabilities $P(J_{t\ell}(\mathrm{s}_i) \leq x)$, given the observed indicator of the previous day, for a set of discrete values $x = 0, 1, 2, \ldots$ (in °C). Using the previously described out-of-sample method, we generate samples of increments for the sites omitted from estimation, for each day on which a record was observed at those sites, and conditional on the observed value of $I_{t,\ell-1}(\mathrm{s}_i)$. Given a generated sample, we can obtain one observation of the proportion of increments lower than or equal to x across the considered period,

$$\frac{1}{N(\mathrm{s}_i)} \sum_{(t,\ell)\in\mathcal{A}_1(\mathrm{s}_i)} 1(J_{t\ell}(\mathrm{s}_i) \leq x),$$

where $1(\cdot)$ denotes the indicator variable of an event, $\mathcal{A}_1(\mathrm{s}_i) = \{(t,\ell) \in \mathcal{T} \times \mathcal{L} : I_{t\ell}(\mathrm{s}_i) = 1\}$ denotes the set of days with a record at s_i, and $N(\mathrm{s}_i) = \sum_{(t,\ell)\in\mathcal{T}\times\mathcal{L}} I_{t\ell}(\mathrm{s}_i)$ is its size, i.e., the total number of records at s_i. If we generate B samples of increments, we obtain a sample of B observations of the proportions for each x, and then the corresponding posterior mean and 95% CI. Using the observed sample, we calculate the empirical counterpart. Figure 4 summarizes the posterior means, the CIs of the proportions for $x = 0, 1, 2, \ldots$ (in °C) together with the empirical counterparts for four illustrative sites in the last 30 years, the period 1992–2021. These four sites represent different areas and climates of the peninsula. Bilbao, on the northern Cantabrian coast, has a humid Atlantic climate, Huelva, on the southern coast, features a Mediterranean climate; Daroca and Vitoria are both inland locations, but the former has a continental-Mediterranean climate, while the latter has a continental climate with Atlantic influence. The results show that the predictive CIs capture the observed proportions at nearly all 40 sites.

5.3 Analyzing spatial averages

Another key aspect of the model to be validated is its ability to capture behavior over time and the joint spatial behavior. We will assess this by comparing various empirical averages of interest with the corresponding averages from the realizations of the posterior predictive distribution. Since we are computing spatial averages, the out-of-sample validation approach, omitting one station at a time, is no longer feasible. Instead, we will apply a MC method using the model fitted with data from all 40 sites to generate the samples.

First, to characterize the annual evolution across Spain, we compute the spatial average increment for year t across the days in JJA,

$$\bar{J}_t = \frac{1}{N_t} \sum_{(\ell,\mathrm{s}_i)\in\mathcal{A}_{1,t}} J_{t\ell}(\mathrm{s}_i),$$

where $\mathcal{A}_{1,t} = \{(\ell, \mathrm{s}_i) \in \mathcal{L} \times \mathcal{S} : I_{t\ell}(\mathrm{s}_i) = 1\}$ denotes the set of days and sites with a record on year t, and N_t its size, i.e., the number of increments at year t in the 92×40 considered series.

Analogously, replacing the year t with the day ℓ, we compute the spatial average increments for each day ℓ within the year t in the observed period of years 1961–2021,

$$\bar{J}_\ell = \frac{1}{N_\ell} \sum_{(t,\mathrm{s}_i)\in\mathcal{A}_{1,\ell}} J_{t\ell}(\mathrm{s}_i).$$

Figure 5 displays the posterior mean, the 95% CI, and the empirical values of the spatial average increments, $\bar{J}_t$ and

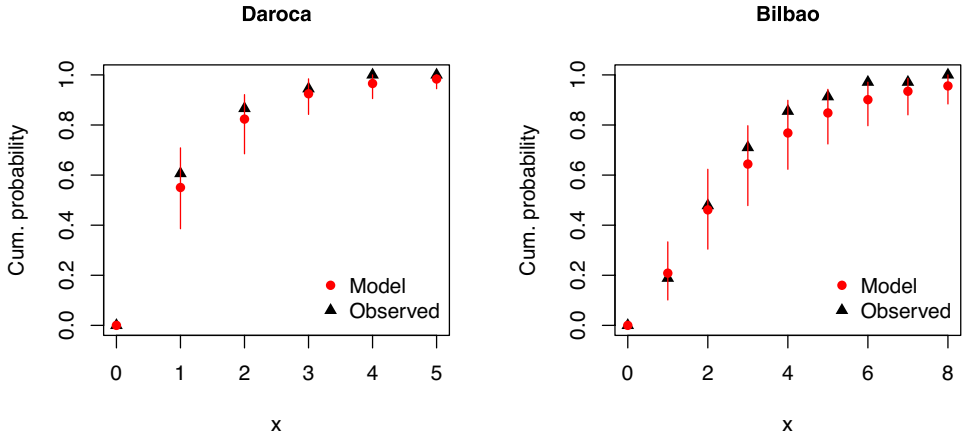

Fig. 4 Posterior mean and 95% CIs obtained of the proportion of increments lower than or equal to x, in °C, in period 1992–2021 obtained from the model using an out-of-sample approach and empirical counterparts, in four illustrative sites

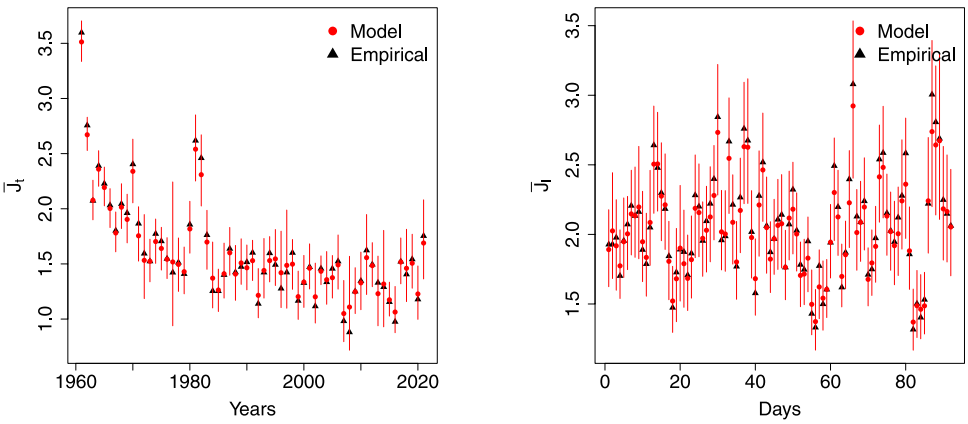

Fig. 5 Posterior mean and 95% CIs of the spatial averages $\bar{J}_t$ (left) and $\bar{J}_\ell$ (right), and corresponding empirical values, in °C

$\bar{J}_\ell$, computed for the observed period 1961–2021. The CIs encompass the empirical values in all cases, and the model effectively captures the observed time trend and also the seasonal behavior within the year, confirming the adequacy of the model to capture these features.

From a descriptive perspective, the results indicate that, as expected, the mean of the increments declines during the early years and stabilizes after the early 1980 s. Interestingly, the seasonal pattern of the increments differs from the seasonal cycle of daily temperatures in Spain, where peak values typically occur in late July and early August (AEMET 2011), providing additional insight into how extreme values evolve differently from seasonal trends in the mean.

6 Post-model inference using Monte Carlo simulation

One important feature of model MS3 is its ability to predict increments at unobserved sites. More specifically, MS3 is a generative model capable of producing samples of increments during the observed period at any location within the study region, using both the conditional and marginal distributions described in Sect. 3. The first step in this process is to obtain the conditional or marginal posterior predictive distribution of increments on the $0.25^\circ \times 0.25^\circ$ grid shown in Fig. 1. These posterior distributions allow direct inference on the increments and, by drawing samples from them, enable the use of MC methods to analyze more complex measures of interest based on the increments.

In this section, we apply this procedure with model MS3 to characterize the temporal evolution of increments both across and within the year for different regions. In addition, the approach allows us to generate maps that describe the spatial behavior of the increments and to quantify the uncertainty associated with these estimators.

6.1 Conditional posterior distribution given the previous day indicator

The conditional distribution, given the previous day's indicator, can be easily derived from the model and serves as a useful tool for evaluating the effect of persistence in the increments. Specifically, it allows us to assess how a record occurrence on the previous day influences the distribution of increments. To achieve this, we compare the posterior predictive distributions when the previous day's indicator is 1 versus 0. For example, we can obtain maps of the posterior mean of the difference between the average increments across all JJA days during a decade D or another period of time, given that the previous day was record-breaking and given it was not,

$$\frac{1}{920}\sum_{t\in D}\sum_{\ell\in JJA}\left[J_{t\ell}(\mathrm{s}) \mid (I_{t,\ell-1}(\mathrm{s})=1) - J_{t\ell}(\mathrm{s}) \mid (I_{t,\ell-1}(\mathrm{s})=0)\right].$$

For illustration, the decade 2012–2021 ($D6$) is presented in Fig. 6. The results indicate that record-breaking days lead to higher temperature increments on the following day. The mean increase is approximately $0.4\,^\circ$C inland, reaching around $0.6\,^\circ$C in some areas along the northern and southern coasts. However, in the northeastern coastal region, the increase is slightly lower, around $0.3\,^\circ$C. A similar pattern is observed during decades $D3$ to $D5$, see maps in Section 5.1 of the Supplementary Material, although the differences are slightly higher in 1982–1991.

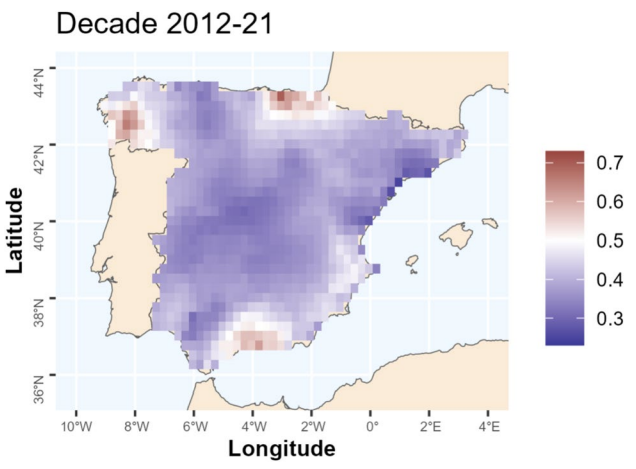

Fig. 6 Posterior mean of the average of the differences between the increments (in °C) given that the previous day was a record and given that it was not, across days in JJA and the last decade

6.2 Marginal posterior distribution

The marginal posterior predictive distribution of the increments is a useful tool for characterizing the behavior of increments over time and across space. It does not require specifying the previous day's indicator but does rely on knowledge of its distribution, specifically, the probability that the previous day was a record. The simplest approach is to estimate this probability using the proportion of the previous day's records, conveniently aggregated by day, year, or region, as appropriate for each context. However, more sophisticated and specific estimators can provide improved results. Here, we use the space-time varying estimators provided by the occurrence model of Castillo-Mateo et al. (2025), although it is important to highlight that any other estimators of the probability of a record could also be applied. This occurrence model consists of a rich Bayesian hierarchical mixed effects logistic regression model for the indicator events which define record-breaking sequences. It includes explicit trend behavior, autoregression, distance to the coast, interactions, and daily spatial random effects.

The resulting marginal posterior distributions are useful to compare and make inference based on MC methods, about the evolution of the increments or their averages in periods of interest both across time and space, as we illustrate in the following sections.

6.2.1 Spatial analysis of increments

To evaluate the spatial differences in the behavior of the increments, we first consider the average of the increments during the three summer months over a decade D at a given point s, $\bar{J}_{D,JJA}(\mathrm{s}) = \sum_{t\in D}\sum_{\ell\in JJA} J_{t\ell}(\mathrm{s})/920$. The maps of the posterior mean, along with the 5th and 95th percentiles of this average increments for the most recent decade,

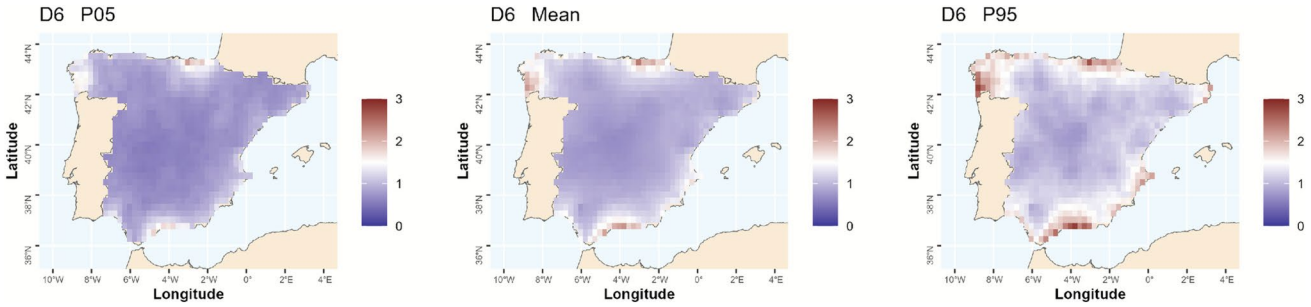

Fig. 7 Posterior mean and 5th and 95th percentiles of the average increments, in °C, over decade 2012–2021

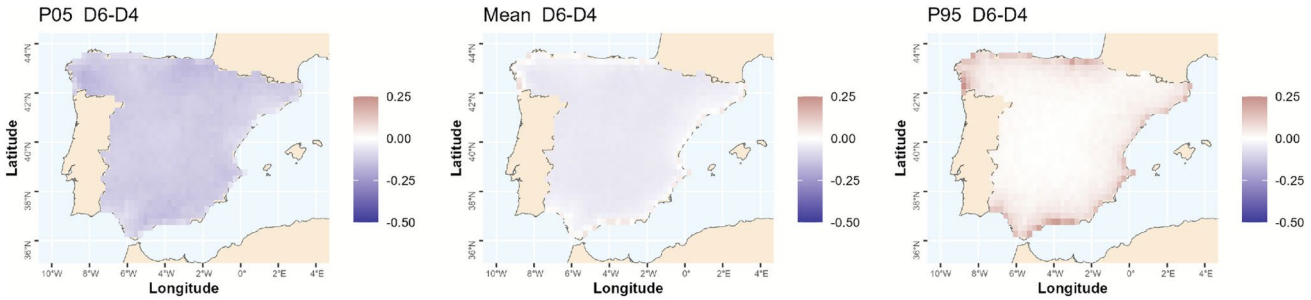

Fig. 8 Posterior mean and 5th and 95th percentiles of $\bar{J}_{D_6,JJA}(\mathrm{s}) - \bar{J}_{D_4,JJA}(\mathrm{s})$, in °C, where $D6$ and $D4$ are the decades 2012–2021 and 1992–2001, respectively

2012–2021, are shown, as an illustration, in Fig. 7. The posterior mean is approximately °C across most of Spain, except in certain coastal areas, including the Basque Country, Galicia in the north, and the southern Mediterranean coast, where the mean approaches 2 °C. In these regions, and more generally in coastal areas, the distribution of average increments is asymmetric, exhibiting a heavier right tail with the 95th percentile showing a greater increase relative to the mean. This pattern aligns with empirical values observed in coastal sites. For instance, the highest observed average increments in the same period occur in San Sebastián, Bilbao, Santander, Santiago, and Coruña, measuring $2.7\,^{\circ}C$, $2.1\,^{\circ}C$, $2.2\,^{\circ}C$, $2.1\,^{\circ}C$, and $1.9\,^{\circ}C$, respectively.

The maps of the mean and the percentiles for decades $D2$ to $D6$ and for the entire period, are shown in Section 5.2 of the Supplementary Material; decade $D1$ is omitted due to high variability in the increments during the early stage. As could be expected, the mean of the increments decreases over the decades: while in $D2$ the mean across most of inland Spain ranges from 1 to 1.5 °C, in $D6$ it ranges from 0.5 to 1 °C. However, the decrease between decades is much smaller in the aforementioned coastal areas.

To better assess the temporal behavior of increments within a spatial framework, we compare average increments across different decades by computing the posterior distribution of their difference, $\bar{J}_{D_1,JJA}(\mathrm{s}) - \bar{J}_{D_2,JJA}(\mathrm{s})$. Figure 8 presents the posterior mean of this difference between the most recent decade (2012–2021) and two decades prior (1992–2001). Although the magnitude of these differences is small, the map highlights some consistent spatial variations over time. While inland regions exhibit a decrease of approximately $0.04\,^{\circ}\mathrm{C}$ in the posterior mean of average increments, coastal areas show an increase of around $0.05\,^{\circ}$ C. Furthermore, given the uncertainty of these differences expressed by the 5th and 95th percentiles, there is no evidence that coastal changes are significantly different from zero, whereas inland regions show a slight decline. Maps showing the differences between each decade and $D6$ are also presented in Section 5.2 of the Supplementary Material. Similar conclusions are obtained in the comparison of all the decades although, inland, larger differences are observed in the earlier decades. However, in none of the cases do the differences along the coast show evidence of being significantly different from zero, supporting the conclusion that the posterior mean of the increments in coastal areas is not decreasing.

Another approach to evaluating spatial and temporal differences in average increments is through probabilities. We use this method to assess whether a seasonal pattern exists within the summer, given that the magnitude of differences during this period is very small. To do this, we compare increments among months. Specifically, we compute the probabilities $P_D\left(\bar{J}_{t,M_1}(\mathrm{s}) > \bar{J}_{t,M_2}(\mathrm{s})\right)$ where $\bar{J}_{t,M}(\mathrm{s})$ is the average increment in month M at year t and the probability is computed over the 10 years t within the decade D. Figure 9 shows the probabilities comparing July and June, August and June, and August and July in the last decade $D6$,

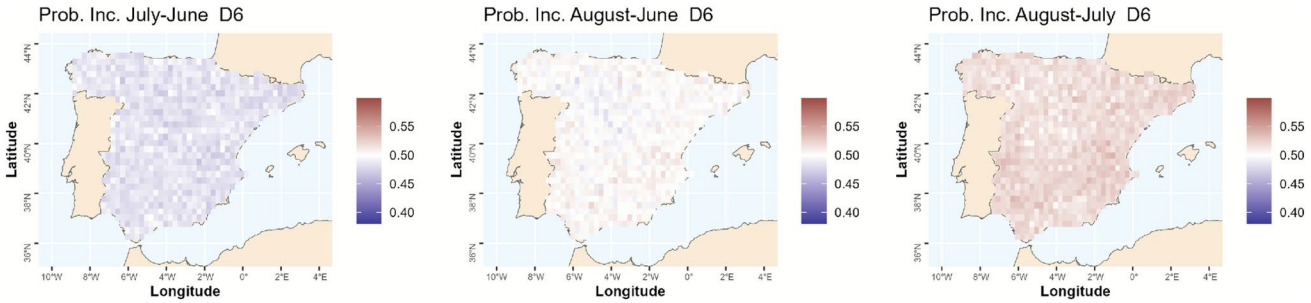

Fig. 9 Probabilities of the average increments in July being higher than in June, and in August being higher than in June and July, over decade *D*6

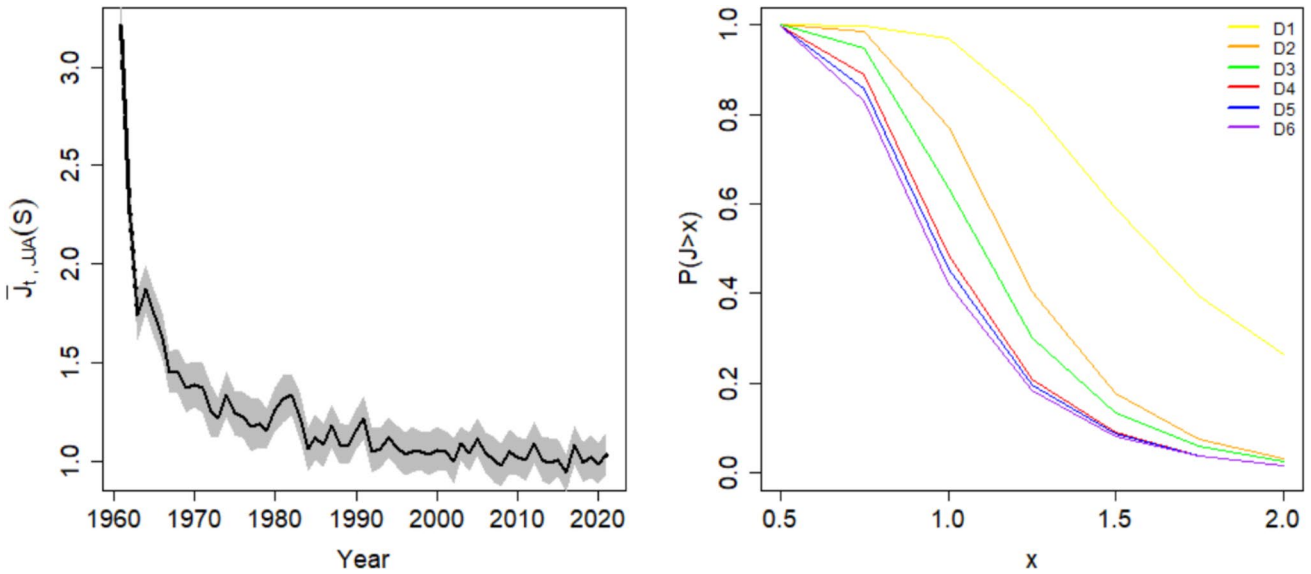

Fig. 10 Left: Posterior mean and the 90% CI of the annual average of the increments, in °C, over peninsular Spain. Right: Posterior mean of $P_{D,G}(\bar{J}_{t,JJA}(\mathrm{s}) > x)$ for different values x, in °C, across the 6 decades

as illustration. The results show that, over the last decade, the probability of the average increment in July tends to be slightly lower than in June and in August. Although the differences are small and some uncertainty exists in the estimations, this result remains spatially consistent. Maps showing the probabilities for decades *D*2 to *D*6 and for the entire period are also presented in Section 5.2 of the Supplementary Material. The behavior across months is not consistent over all the decades. However, the increments in June are generally higher than those in July and August, except during decade *D*3. Notably, this seasonal pattern of the increments, peaking in June, contrasts with the typical summer temperature cycle in Spain, where July and August record the highest temperatures (AEMET 2011). This provides the novel suggestion that extreme temperatures in June are increasing more rapidly than in the rest of the summer.

6.2.2 Time evolution of increments

Our first objective in this section is to characterize the annual evolution of the increments over Spain. Figure 10 shows the posterior mean, and the 90% CI of the annual average of the increments across Spain,

$$\bar{J}_{t,JJA}(G) = \frac{1}{92 \times |G|} \sum_{\ell \in JJA} \sum_{\mathrm{s}_j \in G} J_{t\ell}(\mathrm{s}_j),$$

where G is the grid of points covering peninsular Spain and $|G| = 844$ is the number of points in that grid. As expected, increments in the early years (which correspond mainly to the first records) are higher, but they become more stable over time. After the first 30 years, the mean moves around °C. Although no clear trend has been observed in recent decades, we can assess whether the increments continue to decrease using the probabilities that compare two decades D_A and D_B, $P_G(\bar{J}_{D_A,JJA}(\mathrm{s}) < \bar{J}_{D_B,JJA}(\mathrm{s}))$. The posterior mean of these probabilities for comparing *D*6 and *D*4,

and $D6$ and $D5$ are 0.80 and 0.69, respectively. These results suggest that the increments continue to decrease, although at a progressively slower rate.

Figure 10 (right) compares the posterior mean of $P_{D,G}(\bar{J}_{t,JJA}(\mathrm{s}) > x)$, the probability that the average JJA increment in a given year exceeds x, for different values of x, where the probability is computed over Spain and one decade, for each of the 6 considered decades. The densities of the previous probabilities for two of the values $x = 1\,^\circ$C and $1.5\,^\circ$C are shown in Fig. 11; the results show that while the distribution of the average JJA increments evolves over time, changes occur differently in the tails. Specifically, although the center of the distribution has continued to decrease in recent decades, the upper tail has remained stable over the last 30 years.

Comparison of the time evolution of increments across inland and coastal areas. Some previous results show small differences in the behavior of increments between inland and certain coastal areas, particularly the Basque Country, Galicia, and parts of the southern coast. To assess a potential general difference between inland and coastal behavior, we analyze the average increments over a region on a given day, defined as, $\bar{J}_{t\ell}(G_R) = \sum_{\mathrm{s}_j \in G_R} J_{t\ell}(\mathrm{s}_j)/|G_R|$, where s_j represents the points in a prediction grid G_R covering the region of interest and $|G_R|$ is the total number of such points. Based on these spatial averages, additional temporal averages can be computed, either across days within year and/or across years. Several analyses have been conducted in this regard, including comparisons of annual trends between inland and coastal regions (with inland areas defined as those more than 50 km from the coast) and also distinguishing among three coastal regions (northern, eastern, and southern). However, no significant differences were found; see Section 6 of the Supplementary Material for further illustration.

6.3 Additional inference tools: Cumulative increments across a period of time

An additional advantage of the conditional model J | I proposed in this work is that it can be combined with a model for the occurrence of records to make inference on measures that depend on the joint distribution of record occurrences and their increments, that is the vector (I, J). More precisely, by specifying the factorization $[\mathrm{I} \mid \boldsymbol{\theta}_1][\mathrm{J} \mid \mathrm{I}, \boldsymbol{\theta}_2]$ with $\boldsymbol{\theta}_1$ denoting all of the unknowns in a model for record-breaking indicators, $\boldsymbol{\theta}_2$ denoting all the unknowns in a model for the increment given a record and assuming that $\boldsymbol{\theta}_1$ and $\boldsymbol{\theta}_2$ are different sets of parameters, I and J | I can be modeled separately and their combination yields the joint distribution of $(\mathrm{I},\ \mathrm{J})$.

This joint distribution enables, among others, the quantification of the cumulative increment over a period of time in the record temperature value for a given day of the year at a specific site. It also enables the characterization of the record-breaking value of a series in a given year, provided the temperature value for the first year of the series is available. Note that using the proposed model, since the conditional distribution of the increments $J_{t\ell}(\mathrm{s})$ is $Gamma\,(\mu_{t\ell}(\mathrm{s}), \phi)$ and the temperature increments are conditionally independent given their parameters, the marginal distribution of the cumulative increment during a

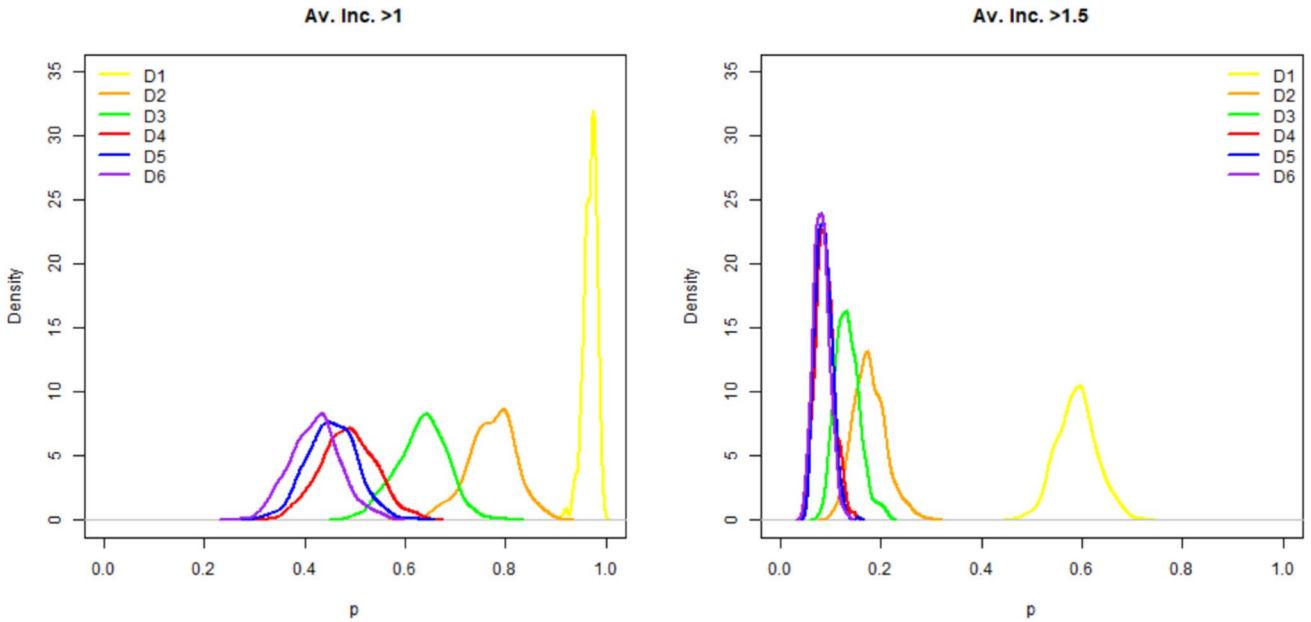

Fig. 11 Densities of the probabilities $P_{D,G}(\bar{J}_{t,JJA}(\mathrm{s}) > x)$ per decades for $x = 1\,^\circ$C and $1.5\,^\circ$C

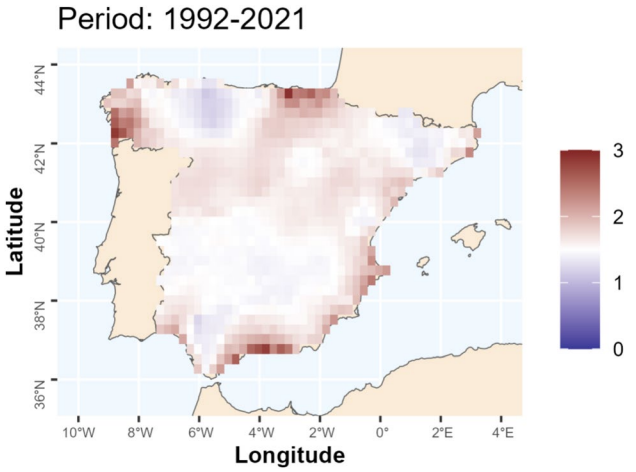

Fig. 12 Posterior mean of the average cumulative increments, in °C, in the last 30 years over the summer months JJA

period of years $\mathcal{T}$ is $Gamma(\sum_{t\in\mathcal{T}_{1,\ell}(\mathrm{s})}\mu_{t\ell}(\mathrm{s}),\phi)$, where $\mathcal{T}_{1,\ell}(\mathrm{s})=\{t\in\mathcal{T}: I_{t\ell}(\mathrm{s})=1\}$. This highlights that distribution of the cumulative increment depends on the distribution of the record indicators.

Given two separate models for I and J | I, we can proceed as follows. First, we generate posterior samples of the record indicators. Next, we generate posterior samples of the increments when a record has occurred. These samples allow us to characterize the posterior distribution of the cumulative increment over a period of years $\mathcal{T}$ given by

$$\sum_{t\in\mathcal{T}_{1,\ell}(\mathrm{s})} J_{t\ell}(\mathrm{s}).$$

Finally, we can illustrate the spatial behavior of the posterior mean of the cumulative increment for a given day or summarize it over a month or a year.

As an illustration, we use posterior samples of the record indicators generated by the model for I of Castillo-Mateo et al. (2025), introduced at the beginning of Section 6.2. However, it is noteworthy that any model capable of generating samples of I can be used in this approach. Figure 12 presents a map of the posterior mean of the average cumulative increments in the last 30 years over the summer months JJA; the cumulative increase of the value of record from 1992 to 2021 in some coastal areas such as Basque country and Galicia is of almost 3 °C, while inland it varies from 1 to 2 °C.

7 Summary and future work

We argue that while explaining the incidence of record-breaking events is important, analyzing the magnitudes of these records also offers valuable insight into the dynamics of daily temperature extremes. To explore this, we propose an approach that does not require modeling the temperature distribution over an entire space-time dataset. Rather, it is sufficient to model the conditional distribution of record values or their increments, i.e., we only need to model the temperature increments given that a record has occurred. This approach has an important advantage: the increments can be treated as conditionally independent and are not constrained by the ordering that affects record values.

Within this framework, we introduce a novel regression model, implemented within a hierarchical Bayesian framework, which analyzes increments across years, by day in the summer season, and by site. This approach allows us to identify covariates that effectively explain the increments, while also assessing variation across time and space (specifically by year, within summer months, and between sites) thereby providing a deeper understanding of the record-breaking process. Importantly, the proposed approach captures the underlying dependencies and heterogeneity that fixed effects cannot explain. Spatial dependence is modeled using spatial Gaussian processes, temporal autocorrelation is addressed through autoregressive random effects, with interactions between spatial and temporal components incorporated as needed.

Another advantage of the proposed model is its ability to characterize both the conditional distribution of the increments, given the previous day's record-breaking indicator, and their marginal distribution, obtained by marginalizing over that indicator. Additionally, it allows for the characterization of the cumulative increment of the record value over a specified period, provided a posterior distribution for the daily record probabilities is available. The Bayesian framework facilitates the use of the increments model and MC simulation for performing a rich range of inference to enable appreciation of spatial variation over the region of study, as well as comparison over the years. This approach yields not only estimates of mean values but also quantifies their uncertainty through the posterior distribution. Furthermore, it supports the derivation of useful inference tools, such as the probabilities of events of interest and the generation of maps displaying either these probabilities, posterior means or other summary measures of parameters of interest.

Conclusions on record increments of daily temperature over Spain. Using data from peninsular Spain, spanning from 1960 to 2021, we conclude that a Gamma model for the increments performs far better than an Exponential model. Our analysis also reveals that key spatial information is captured by the logarithm of elevation and the logarithm of the distance to the coast. Temporal covariates are also essential: a second-order polynomial trend effectively models long-term evolution, while the inclusion of the previous day's record indicator captures serial correlation. The

effects of these time covariates vary spatially so that interaction terms with the logarithm of the distance to the coast are also necessary. Finally, a daily effect with an autoregressive structure is required to account for serial correlation but also for seasonal variation within the summer month and its interannual variability. Using different MC inference tools we conclude:

- The occurrence of a record on the previous day increases the posterior mean of the increment by between 0.3 and 0.6 °C, depending on the region.
- The posterior mean of the average increment on a record-breaking day during the decade 2012–2021 is around 1°C in most inland regions. This value increases to approximately 2 °C in coastal areas, such as the Basque Country, Galicia, and the southern Mediterranean coast.
- Regarding the long-term evolution, as expected, the magnitude and variability of increments decreases over time, with a slower rate of decline after 30 years, that varies around 1°C. Notably, the evolution of the tails differs from that of the bulk of the distribution, with the tails being more stable over the last 30 years.
- Although changes in increment behavior are observed across summer months, they do not align with the typical seasonal pattern of daily temperature; July, for instance, has shown the lowest average increments over the past decade across peninsular Spain.
- The cumulative increment in record values from 1992 to 2021 reaches nearly 3 °C in the most affected coastal regions, while inland areas show cumulative values ranging from 1 to 2 °C.*Future work.* Since our work is applicable to general daily temperature datasets, or even other environmental series, users may readily apply it to other spatial domains. Also, our model is a mean model. If interest was, perhaps, in extremes of increments, our models could be modified to quantile regression specifications. Finally, if our temperature data provided daily maximum temperatures and daily minimum temperatures, we could offer different definitions of record breaking and therefore different realizations of increments. Following our ideas here, we could develop modeling for these increments.

Supplementary Information The online version contains supplementary material available at https://doi.org/10.1007/s00477-025-03159-x.

Acknowledgements This work was supported by MCIN/AEI/10.13039/501100011033 and Unión Europea NextGenerationEU under Grants TED2021-130702B-I00, and PID2023-150234NB-I00, and Gobierno de Aragón under Research Group E46_23R: Modelos Estocásticos and research project PROY_T21_24-HIDROGIF.

Author contributions All authors contributed to the conception and revision of this manuscript. A.C. implemented the analyses. All authors have read and approved the final version of the article.

Funding Open Access funding provided thanks to the CRUE-CSIC agreement with Springer Nature. Open access funding provided thanks to the CRUE-CSIC agreement with Springer Nature

Data availability The dataset and R code/functions used in this manuscript are publicly available at the following GitHub repository: https://github.com/anaccebrian/RecordIncrements/

Declarations

Conflict of interest The authors declare no competing interests.

References

AEMET (2011) Atlas climático ibérico/iberian climate atlas. Tech. rep., Agencia Estatal de Meteorología. Madrid, Spain, https://doi.org/10.31978/784-11-002-5

Arnold BC, Balakrishnan N, Nagaraja HN (1998) Records. Wiley series in probability and statistics, John, New York. https://doi.org/10.1002/9781118150412

Castillo-Mateo J, Asín J, Cebrián AC, Gelfand AE, Abaurrea J (2023) Spatial quantile autoregression for season within year daily maximum temperature data. Annal Appl Stat 17(3):2305–2325. https://doi.org/10.1214/22-AOAS1719

Castillo-Mateo J, Gelfand AE, Gracia-Tabuenca Z, Asín J, Cebrián AC (2025) Spatio-temporal modeling for record-breaking temperature events in Spain. J Am Stat Assoc 120(550):645–657. https://doi.org/10.1080/01621459.2024.2427430

Chen SX (1999) Beta kernel estimators for density functions. Comput Stat Data Anal 31(2):131–145

Coles S (2001) An introduction to statistical modeling of extreme values. Springer Series in Statistics, Springer, London

Coumou D, Robinson A, Rahmstorf S (2013) Global increase in record-breaking monthly-mean temperatures. Clim Change 118(3–4):771–782. https://doi.org/10.1007/s10584-012-0668-1

Elguindi N, Rauscher SA, Giorgi F (2013) Historical and future changes in maximum and minimum temperature records over Europe. Clim Change 117:415–431. https://doi.org/10.1007/s10584-012-0528-z

Jiang N, Zhu C, Hu ZZ, McPhaden MJ, Chen D, Liu B, Ma S, Yan Y, Zhou T, Qian W et al (2024) Enhanced risk of record-breaking regional temperatures during the 2023–24 El Niño. Sci Rep 14(1):2521

Keellings D, Waylen P (2015) Investigating teleconnection drivers of bivariate heat waves in Florida using extreme value analysis. Clim Dyn 44(11):3383–3391

Klein Tank AMG, Wijngaard JB, Können GP, Böhm R, Demarée G, Gocheva A, Mileta M, Pashiardis S, Hejkrlik L, Kern-Hansen C, Heino R, Bessemoulin P, Müller-Westermeier G, Tzanakou M, Szalai S, Pálsdóttir T, Fitzgerald D, Rubin S, Capaldo M, Petrovic P (2002) Daily dataset of 20th-century surface air temperature and precipitation series for the European Climate Assessment. Int J Climatol 22(12):1441–1453. https://doi.org/10.1002/joc.773

Lehmann J, Coumou D, Frieler K (2015) Increased record-breaking precipitation events under global warming. Clim Change 132(4):501–515. https://doi.org/10.1007/s10584-015-1434-y

Lehmann J, Mempel F, Coumou D (2018) Increased occurrence of record-wet and record-dry months reflect changes in mean rainfall. Geophys Res Lett 45(24):13468–13476. https://doi.org/10.1029/2018GL079439

Lindgren F, Bolin D, Rue H (2022) The SPDE approach for Gaussian and non-Gaussian fields: 10 years and still running. Spatial Stat 50:100599

Newman WI, Malamud BD, Turcotte DL (2010) Statistical properties of record-breaking temperatures. Phys Rev E-Statist Nonlinear Soft Matter Phys 82(6):066111

Pan Z, Wan B, Gao Z (2013) Asymmetric and heterogeneous frequency of high and low record-breaking temperatures in China as an indication of warming climate becoming more extreme. J Geophys Res Atmos 118(12):6152–6164. https://doi.org/10.1002/jgrd.50467

Rahmstorf S, Coumou D (2011) Increase of extreme events in a warming world. Proc Natl Acad Sci 108(44):17905–17909. https://doi.org/10.1073/pnas.1101766108

Rue H, Martino S, Chopin N (2009) Approximate Bayesian inference for latent Gaussian models by using integrated nested Laplace approximations. J Royal Stat Soc Ser B (Statistical Methodology) 71(2):319–392. https://doi.org/10.1111/j.1467-9868.2008.00700.x

Rue H, Riebler A, et al. (2024) R-INLA: Bayesian computing with INLA. https://www.r-inla.org, R package version 24.6.27

Schliep EM, Gelfand AE, Abaurrea J, Asín J, Beamonte MA, Cebrián AC (2021) Long-term spatial modelling for characteristics of extreme heat events. J R Stat Soc Ser A Stat Soc 184(3):1070–1092

Shaby BA, Reich BJ, Cooley D, Kaufman CG (2016) A Markov-switching model for heat waves. Annal Appl Stat 10(1):74–93. https://doi.org/10.1214/15-AOAS873

Sousa PM, Barriopedro D, Ramos AM, García-Herrera R, Espírito-Santo F, Trigo RM (2019) Saharan air intrusions as a relevant mechanism for Iberian heatwaves: the record breaking events of August 2018 and June 2019. Weather Clim Extremes 26:100224. https://doi.org/10.1016/j.wace.2019.100224

Tian P, Zhang F, Yan Y, Liu Y, Zhang H, Li J (2025) Spatial inequalities in global population exposure to extreme heats and heatwaves. Appl Geogr 174:103474

Wergen G, Hense A, Krug J (2014) Record occurrence and record values in daily and monthly temperatures. Clim Dyn 42(5):1275–1289. https://doi.org/10.1007/s00382-013-1693-0

Yang X, Xu X, Wang Y, Yang J, Wu X (2024) Heat exposure impacts on urban health: a meta-analysis. Sci Total Environ 947:174650. https://doi.org/10.1016/j.scitotenv.2024.174650